

Superfluidity in Neutron-Star Crusts Within the Nuclear Energy Density Functional Theory

OUTER LAYER
1 meter thick
solid or liquid

CORE
10-15 kilometer deep
liquid

Nicolas Chamel

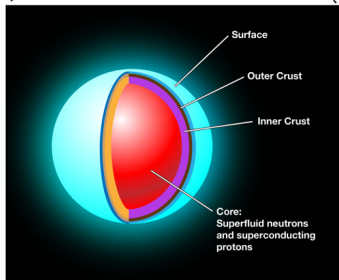
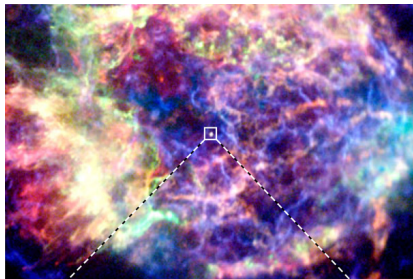
Institute of Astronomy and Astrophysics
Université Libre de Bruxelles, Belgium

in collaboration with:
S. Goriely, J. M. Pearson, A. F. Fantina, A. Pastore



CRUST
1 kilometer thick
solid

Punchline

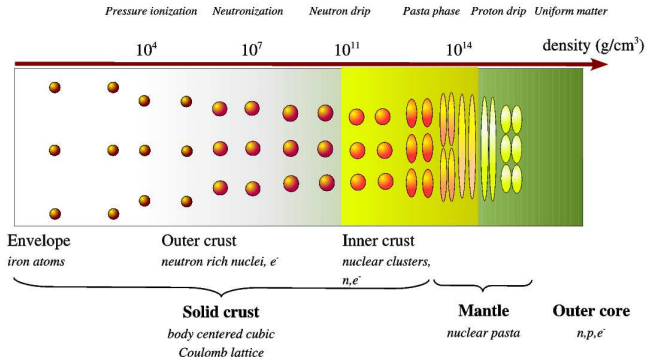


Superfluidity in the crust of a neutron star may leave its imprint on various observed astrophysical phenomena, such as

- pulsar sudden spin-ups (frequency 'glitches'),
- thermal relaxation in transiently accreting neutron stars,
- quasiperiodic oscillations in magnetars.

Prelude

The inner crust of a neutron star is made of neutron-proton clusters immersed in a neutron liquid. The average density is rather low (about half saturation density at most), but matter is inhomogeneous.



Chamel&Haensel, *Living Reviews in Relativity* 11 (2008), 10
<http://relativity.livingreviews.org/Articles/lrr-2008-10/>

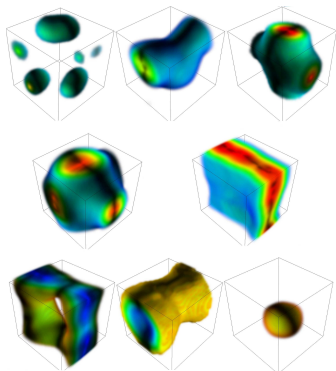
Superfluidity in neutron-star crusts: theoretical challenges

Describing superfluidity in neutron-star crusts requires a unified understanding of nuclear pairing in both atomic nuclei and infinite homogeneous nuclear matter.

Because of inhomogeneities, microscopic calculations based on realistic interactions are currently not feasible.

State-of-the-art calculations rely on the self-consistent nuclear energy density functional (EDF) theory.

This EDF theory provides a consistent and numerically tractable treatment of nuclear clusters and unbound neutrons.



Outline

- 1 Nuclear energy density functionals for astrophysics
 - ▷ nuclear energy density functional theory
 - ▷ fitting protocols of the Brussels-Montreal functionals
 - ▷ towards a better treatment of nuclear pairing (BSk16-32)

- 2 Applications to neutron-star crusts
 - ▷ role of nuclear pairing on the equilibrium composition
 - ▷ neutron superfluidity
 - ▷ collective excitations

Nuclear energy density functional theory in a nut shell

The energy E is expressed as a *functional* of the “**normal**” and “**abnormal**” density matrices:

$$n_q(\mathbf{r}, \sigma; \mathbf{r}', \sigma') = \langle \Psi | c_q(\mathbf{r}'\sigma')^\dagger c_q(\mathbf{r}\sigma) | \Psi \rangle,$$
$$\tilde{n}_q(\mathbf{r}, \sigma; \mathbf{r}', \sigma') = -\sigma' \langle \Psi | c_q(\mathbf{r}' - \sigma') c_q(\mathbf{r}\sigma) | \Psi \rangle$$

where $c_q(\mathbf{r}\sigma)^\dagger$ and $c_q(\mathbf{r}\sigma)$ are the creation and destruction operators for nucleon of type q ($q = n, p$ for neutrons, protons) at position \mathbf{r} with spin σ ($\sigma = \pm 1$ for spin up and down).

Nuclear energy density functional theory in a nut shell

The energy E is expressed as a *functional* of the “**normal**” and “**abnormal**” density matrices:

$$n_q(\mathbf{r}, \sigma; \mathbf{r}', \sigma') = \langle \Psi | c_q(\mathbf{r}'\sigma')^\dagger c_q(\mathbf{r}\sigma) | \Psi \rangle,$$
$$\tilde{n}_q(\mathbf{r}, \sigma; \mathbf{r}', \sigma') = -\sigma' \langle \Psi | c_q(\mathbf{r}' - \sigma') c_q(\mathbf{r}\sigma) | \Psi \rangle$$

where $c_q(\mathbf{r}\sigma)^\dagger$ and $c_q(\mathbf{r}\sigma)$ are the creation and destruction operators for nucleon of type q ($q = n, p$ for neutrons, protons) at position \mathbf{r} with spin σ ($\sigma = \pm 1$ for spin up and down).

In turn the density matrices can be expressed in terms of the **quasiparticle wave functions** $\varphi_{1k}^{(q)}(\mathbf{r})$ and $\varphi_{2k}^{(q)}(\mathbf{r})$ as

$$n_q(\mathbf{r}, \sigma; \mathbf{r}', \sigma') = \sum_{k(q)} \varphi_{2k}^{(q)}(\mathbf{r}, \sigma) \varphi_{2k}^{(q)}(\mathbf{r}', \sigma')^*$$
$$\tilde{n}_q(\mathbf{r}, \sigma; \mathbf{r}', \sigma') = - \sum_{k(q)} \varphi_{2k}^{(q)}(\mathbf{r}, \sigma) \varphi_{1k}^{(q)}(\mathbf{r}', \sigma')^* = - \sum_k \varphi_{1k}^{(q)}(\mathbf{r}, \sigma) \varphi_{2k}^{(q)}(\mathbf{r}', \sigma')^*.$$

Nuclear energy density functional theory in a nut shell

The energy E is expressed as a *functional* of the “**normal**” and “**abnormal**” density matrices:

$$n_q(\mathbf{r}, \sigma; \mathbf{r}', \sigma') = \langle \Psi | c_q(\mathbf{r}'\sigma')^\dagger c_q(\mathbf{r}\sigma) | \Psi \rangle,$$
$$\tilde{n}_q(\mathbf{r}, \sigma; \mathbf{r}', \sigma') = -\sigma' \langle \Psi | c_q(\mathbf{r}' - \sigma') c_q(\mathbf{r}\sigma) | \Psi \rangle$$

where $c_q(\mathbf{r}\sigma)^\dagger$ and $c_q(\mathbf{r}\sigma)$ are the creation and destruction operators for nucleon of type q ($q = n, p$ for neutrons, protons) at position \mathbf{r} with spin σ ($\sigma = \pm 1$ for spin up and down).

In turn the density matrices can be expressed in terms of the **quasiparticle wave functions** $\varphi_{1k}^{(q)}(\mathbf{r})$ and $\varphi_{2k}^{(q)}(\mathbf{r})$ as

$$n_q(\mathbf{r}, \sigma; \mathbf{r}', \sigma') = \sum_{k(q)} \varphi_{2k}^{(q)}(\mathbf{r}, \sigma) \varphi_{2k}^{(q)}(\mathbf{r}', \sigma')^*$$
$$\tilde{n}_q(\mathbf{r}, \sigma; \mathbf{r}', \sigma') = - \sum_{k(q)} \varphi_{2k}^{(q)}(\mathbf{r}, \sigma) \varphi_{1k}^{(q)}(\mathbf{r}', \sigma')^* = - \sum_k \varphi_{1k}^{(q)}(\mathbf{r}, \sigma) \varphi_{2k}^{(q)}(\mathbf{r}', \sigma')^*.$$

The *exact* ground-state energy can be obtained by minimizing the energy functional $E[n_q(\mathbf{r}, \sigma; \mathbf{r}', \sigma'), \tilde{n}_q(\mathbf{r}, \sigma; \mathbf{r}', \sigma')]$ under the constraint of fixed nucleon numbers.

Nuclear energy density functional theory in a nut shell

In the simplest cases, E is written as the integral of a *local* functional

$$E = \int \mathcal{E} \left[n_q(\mathbf{r}), \nabla n_q(\mathbf{r}), \tau_q(\mathbf{r}), \mathbf{J}_q(\mathbf{r}), \tilde{n}_q(\mathbf{r}) \right] d^3\mathbf{r}$$

where

$$\begin{aligned} n_q(\mathbf{r}) &= \sum_{\sigma=\pm 1} n_q(\mathbf{r}, \sigma; \mathbf{r}, \sigma) \\ \tau_q(\mathbf{r}) &= \sum_{\sigma=\pm 1} \int d^3\mathbf{r}' \delta(\mathbf{r} - \mathbf{r}') \nabla \cdot \nabla' n_q(\mathbf{r}, \sigma; \mathbf{r}', \sigma) \\ \mathbf{J}_q(\mathbf{r}) &= -i \sum_{\sigma, \sigma'=\pm 1} \int d^3\mathbf{r}' \delta(\mathbf{r} - \mathbf{r}') \nabla n_q(\mathbf{r}, \sigma; \mathbf{r}', \sigma') \times \boldsymbol{\sigma}_{\sigma'\sigma} \\ \tilde{n}_q(\mathbf{r}) &= \sum_{\sigma=\pm 1} \tilde{n}_q(\mathbf{r}, \sigma; \mathbf{r}, \sigma) \end{aligned}$$

and $\boldsymbol{\sigma}_{\sigma\sigma'}$ denotes the Pauli spin matrices.

Duguet, Lecture Notes in Physics 879 (Springer-Verlag, 2014), p. 293

Dobaczewski & Nazarewicz, in "50 years of Nuclear BCS" (World Scientific Publishing, 2013), pp.40-60

Nuclear energy density functional theory in a nut shell

Minimizing $E \left[\varphi_{1k}^{(q)}(\mathbf{r}), \varphi_{2k}^{(q)}(\mathbf{r}) \right]$ under the constraint of fixed nucleon numbers leads to the **Hartree-Fock-Bogoliubov** equations:

$$\sum_{\sigma'} \begin{pmatrix} h_q(\mathbf{r})_{\sigma\sigma'} & \Delta_q(\mathbf{r})\delta_{\sigma\sigma'} \\ \Delta_q(\mathbf{r})\delta_{\sigma\sigma'} & -h_q(\mathbf{r})_{\sigma\sigma'} \end{pmatrix} \begin{pmatrix} \varphi_{1k}^{(q)}(\mathbf{r}, \sigma') \\ \varphi_{2k}^{(q)}(\mathbf{r}, \sigma') \end{pmatrix} = E_k \begin{pmatrix} \varphi_{1k}^{(q)}(\mathbf{r}, \sigma) \\ \varphi_{2k}^{(q)}(\mathbf{r}, \sigma) \end{pmatrix}$$

$$h_q(\mathbf{r})_{\sigma'\sigma} \equiv -\nabla \cdot \frac{\delta E}{\delta \tau_q(\mathbf{r})} \nabla \delta_{\sigma\sigma'} + \frac{\delta E}{\delta n_q(\mathbf{r})} \delta_{\sigma\sigma'} - i \frac{\delta E}{\delta \mathbf{J}_q(\mathbf{r})} \cdot \nabla \times \boldsymbol{\sigma}_{\sigma'\sigma} - \mu_q \delta_{\sigma\sigma'},$$

μ_q are the nucleon chemical potentials,

$$\Delta_q(\mathbf{r}) \equiv \frac{\delta E}{\delta \tilde{n}_q(\mathbf{r})} \text{ is called the pair potential or the pairing field.}$$

With suitable boundary conditions, these equations can not only describe the bulk neutron superfluid in neutron-star crusts, but also quantized vortices.

Effective nuclear energy density functional

- **In principle, the nuclear functional could be inferred from realistic interactions** (i.e. fitted to experimental NN phase shifts) using many-body methods

$$\mathcal{E} = \frac{\hbar^2}{2M}(\tau_n + \tau_p) + A(n_n, n_p) + B(n_n, n_p)\tau_n + B(n_p, n_n)\tau_p$$

$$+ C(n_n, n_p)(\nabla n_n)^2 + C(n_p, n_n)(\nabla n_p)^2 + D(n_n, n_p)(\nabla n_n) \cdot (\nabla n_p)$$

+ Coulomb, spin-orbit and pairing

Drut, Furnstahl and Platter, Prog.Part.Nucl.Phys.64(2010)120.

Effective nuclear energy density functional

- **In principle, the nuclear functional could be inferred from realistic interactions** (i.e. fitted to experimental NN phase shifts) using many-body methods

$$\mathcal{E} = \frac{\hbar^2}{2M}(\tau_n + \tau_p) + A(n_n, n_p) + B(n_n, n_p)\tau_n + B(n_p, n_n)\tau_p$$

$$+ C(n_n, n_p)(\nabla n_n)^2 + C(n_p, n_n)(\nabla n_p)^2 + D(n_n, n_p)(\nabla n_n) \cdot (\nabla n_p)$$

+ Coulomb, spin-orbit and pairing

Drut, Furnstahl and Platter, Prog.Part.Nucl.Phys.64(2010)120.

- **But this is a very difficult task** so in practice, phenomenological functionals are employed.
Bender, Heenen and Reinhard, Rev.Mod.Phys.75, 121 (2003).
Bulgac in "50 years of Nuclear BCS" (World Scientific Publishing, 2013), pp.100-110

Effective nucleon-nucleon interactions

Semi-local functionals can be constructed from Skyrme **effective nucleon-nucleon interactions** of the form

$$v_{ij} = t_0(1 + x_0 P_\sigma)\delta(\mathbf{r}_{ij}) + \frac{1}{2}t_1(1 + x_1 P_\sigma)\frac{1}{\hbar^2} [\mathbf{p}_{ij}^2 \delta(\mathbf{r}_{ij}) + \delta(\mathbf{r}_{ij}) \mathbf{p}_{ij}^2] \\ + t_2(1 + x_2 P_\sigma)\frac{1}{\hbar^2}\mathbf{p}_{ij}\cdot\delta(\mathbf{r}_{ij})\mathbf{p}_{ij} + \frac{1}{6}t_3(1 + x_3 P_\sigma)\rho(\mathbf{r})^\alpha \delta(\mathbf{r}_{ij}) \\ + \frac{i}{\hbar^2}W_0(\boldsymbol{\sigma}_i + \boldsymbol{\sigma}_j) \cdot \mathbf{p}_{ij} \times \delta(\mathbf{r}_{ij})\mathbf{p}_{ij}$$

using the “**mean-field**” **approximation**, where $\mathbf{r}_{ij} = \mathbf{r}_i - \mathbf{r}_j$, $\mathbf{r} = (\mathbf{r}_i + \mathbf{r}_j)/2$, $\mathbf{p}_{ij} = -i\hbar(\nabla_i - \nabla_j)/2$ is the relative momentum, and P_σ is the two-body spin-exchange operator.

The parameters t_i , x_i , α , W_0 are fitted to some experimental and/or microscopic nuclear data.

Remark: fitting directly the energy functional \mathcal{E} (to nuclear-matter calculations for instance) may lead to self-interaction errors.

Chamel, Phys. Rev. C 82, 061307(R) (2010).

Brussels-Montreal Skyrme functionals (BSk)

These functionals were fitted to both experimental data and N-body calculations using realistic forces.

Experimental data:

- all atomic masses with $Z, N \geq 8$ from the Atomic Mass Evaluation (root-mean square deviation: 0.5-0.6 MeV)

<http://www.astro.ulb.ac.be/bruslib/>

- charge radii
- incompressibility $K_V = 240 \pm 10$ MeV (ISGMR)
Colò et al., Phys.Rev.C70, 024307 (2004).

N-body calculations using realistic forces:

- equation of state of pure neutron matter
- 1S_0 pairing gaps in nuclear matter
- effective masses in nuclear matter

Phenomenological corrections for atomic nuclei

For atomic nuclei, we add the following corrections to the HFB energy:

- Wigner energy

$$E_W = V_W \exp \left\{ -\lambda \left(\frac{N-Z}{A} \right)^2 \right\} + V'_W |N-Z| \exp \left\{ -\left(\frac{A}{A_0} \right)^2 \right\}$$

$$V_W \sim -2 \text{ MeV}, V'_W \sim 1 \text{ MeV}, \lambda \sim 300 \text{ MeV}, A_0 \sim 20$$

- rotational and vibrational spurious collective energy

$$E_{\text{coll}} = E_{\text{rot}}^{\text{crank}} \left\{ b \tanh(c|\beta_2|) + d|\beta_2| \exp\{-l(|\beta_2| - \beta_2^0)^2\} \right\}$$

This latter correction was shown to be in good agreement with calculations using 5D collective Hamiltonian.

Goriely, Chamel, Pearson, Phys.Rev.C82,035804(2010).

In this way, these collective effects do not contaminate the parameters (≤ 20) of the functional.

Brussels-Montreal Skyrme functionals

Main features of the latest functionals:

Chamel et al., Acta Phys. Pol. B46, 349(2015)

- ▶ **fit to realistic 1S_0 pairing gaps (no self-energy)** (BSk16-17)
Chamel, Goriely, Pearson, Nucl.Phys.A812,72 (2008)
Goriely, Chamel, Pearson, PRL102,152503 (2009).
- ▶ **removal of spurious spin-isospin instabilities** (BSk18)
Chamel, Goriely, Pearson, Phys.Rev.C80,065804(2009)
- ▶ **fit to realistic neutron-matter equation of state** (BSk19-21)
Goriely, Chamel, Pearson, Phys.Rev.C82,035804(2010)
- ▶ **fit to different symmetry energies** (BSk22-26)
Goriely, Chamel, Pearson, Phys.Rev.C88,024308(2013)
- ▶ **optimal fit of the 2012 AME** - rms 0.512 MeV (BSk27*)
Goriely, Chamel, Pearson, Phys.Rev.C88,061302(R)(2013)
- ▶ **generalized spin-orbit coupling** (BSk28-29)
Goriely, Nucl.Phys.A933,68(2015).
- ▶ **fit to realistic 1S_0 pairing gaps with self-energy** (BSk30-32)
Goriely, Chamel, Pearson, to appear in Phys.Rev. C

Empirical pairing energy density functionals

The pairing functional is generally assumed to be local and very often parametrized as

$$E_{\text{pair}} = \int d^3r \mathcal{E}_{\text{pair}}(\mathbf{r}), \quad \mathcal{E}_{\text{pair}} = \frac{1}{4} \sum_{q=n,p} v^{\pi q}[n_n, n_p] \tilde{n}_q^2$$

$$v^{\pi q}[n_n, n_p] = V_{\pi q}^{\Lambda} \left(1 - \eta_q \left(\frac{n}{n_0} \right)^{\alpha_q} \right)$$

with a suitable cutoff prescription (regularization).

Bertsch & Esbensen, Ann. Phys. 209, 327 (1991).

$V_{\pi q}^{\Lambda}$ is usually fitted to the average gap in ^{120}Sn . However, this does not allow for an unambiguous determination of η_q and α_q . Systematic studies of nuclei seem to favor $\eta_q \sim 0.5$ and $0.5 \lesssim \alpha_q \lesssim 1$.

Empirical pairing energy density functionals

The pairing functional is generally assumed to be local and very often parametrized as

$$E_{\text{pair}} = \int d^3r \mathcal{E}_{\text{pair}}(\mathbf{r}), \quad \mathcal{E}_{\text{pair}} = \frac{1}{4} \sum_{q=n,p} v^{\pi q}[n_n, n_p] \tilde{n}_q^2$$
$$v^{\pi q}[n_n, n_p] = V_{\pi q}^{\Lambda} \left(1 - \eta_q \left(\frac{n}{n_0} \right)^{\alpha_q} \right)$$

with a suitable cutoff prescription (regularization).

Bertsch & Esbensen, Ann. Phys. 209, 327 (1991).

$V_{\pi q}^{\Lambda}$ is usually fitted to the average gap in ^{120}Sn . However, this does not allow for an unambiguous determination of η_q and α_q . Systematic studies of nuclei seem to favor $\eta_q \sim 0.5$ and $0.5 \lesssim \alpha_q \lesssim 1$.

Drawbacks for astrophysical applications

This kind of functionals do not have enough flexibility to fit realistic pairing gaps in finite nuclei and in infinite nuclear matter.

Pairing functionals from nuclear-matter calculations

Instead of postulating a specific form for $v^{\pi q}[n_n, n_p]$, we fit *exactly* realistic 1S_0 pairing gaps $\Delta_q(n_n, n_p)$ in infinite homogeneous nuclear matter for each densities n_n and n_p .

Pairing functionals from nuclear-matter calculations

Instead of postulating a specific form for $v^{\pi q}[n_n, n_p]$, we fit *exactly* realistic 1S_0 pairing gaps $\Delta_q(n_n, n_p)$ in infinite homogeneous nuclear matter for each densities n_n and n_p .

Inverting the HFB equations in nuclear matter for a *given* pairing gap function Δ_q thus yields (s.p. energy cutoff ε_Λ above the Fermi level):

$$v^{\pi q} = -8\pi^2 \left(\frac{\hbar^2}{2M_q^*} \right)^{3/2} \left(\int_0^{\mu_q + \varepsilon_\Lambda} \frac{\sqrt{\varepsilon} d\varepsilon}{\sqrt{(\varepsilon - \mu_q)^2 + \Delta_q^2}} \right)^{-1}$$
$$\frac{\hbar^2}{2M_q^*} \equiv \frac{\delta E}{\delta \tau_q}$$

Chamel, Goriely, Pearson, *Nucl. Phys.A812,72 (2008)*.

Analytical expression of the pairing strength

In the “weak-coupling approximation” $\Delta_q \ll \mu_q$ and $\Delta_q \ll \varepsilon_\Lambda$,

$$v^{\pi q} = -\frac{8\pi^2}{\sqrt{\mu_q}} \left(\frac{\hbar^2}{2M_q^*} \right)^{3/2} \left[2 \log \left(\frac{2\mu_q}{\Delta_q} \right) + \Lambda \left(\frac{\varepsilon_\Lambda}{\mu_q} \right) \right]^{-1}$$

$$\Lambda(x) = \log(16x) + 2\sqrt{1+x} - 2 \log \left(1 + \sqrt{1+x} \right) - 4$$

$$\mu_q = \frac{\hbar^2}{2M_q^*} (3\pi^2 n_q)^{2/3}$$

Chamel, Phys. Rev. C 82, 014313 (2010)

Analytical expression of the pairing strength

In the “weak-coupling approximation” $\Delta_q \ll \mu_q$ and $\Delta_q \ll \varepsilon_\Lambda$,

$$v^{\pi q} = -\frac{8\pi^2}{\sqrt{\mu_q}} \left(\frac{\hbar^2}{2M_q^*} \right)^{3/2} \left[2 \log \left(\frac{2\mu_q}{\Delta_q} \right) + \Lambda \left(\frac{\varepsilon_\Lambda}{\mu_q} \right) \right]^{-1}$$

$$\Lambda(x) = \log(16x) + 2\sqrt{1+x} - 2 \log \left(1 + \sqrt{1+x} \right) - 4$$

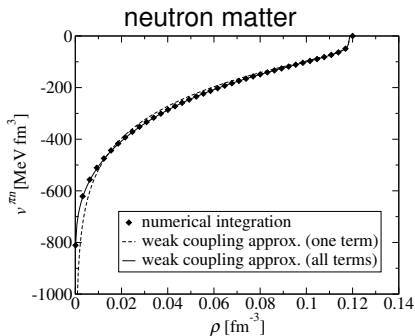
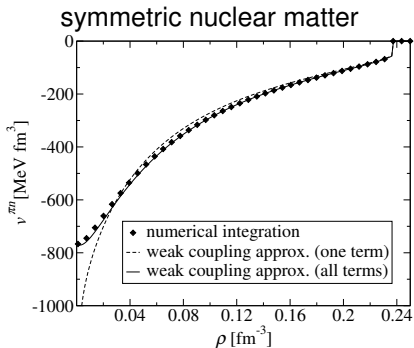
$$\mu_q = \frac{\hbar^2}{2M_q^*} (3\pi^2 n_q)^{2/3}$$

Chamel, Phys. Rev. C 82, 014313 (2010)

- **one-to-one correspondence** between pairing in nuclei and homogeneous nuclear matter
- **no free parameters** apart from the cutoff
- **automatic renormalization** of the pairing strength with ε_Λ

Accuracy of the weak-coupling approximation

This approximation remains very accurate at low densities because the s.p. density of states is not replaced by a constant as in the usual “weak-coupling approximation”. Example with HFB-17:



Chamel, *Phys. Rev. C* 82, 014313 (2010)

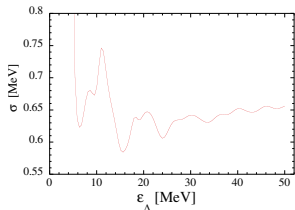
Pairing cutoff and experimental phase shifts

In the limit of vanishing density, the pairing strength

$$v^{\pi q}[n_n, n_p \rightarrow 0] = -\frac{4\pi^2}{\sqrt{\varepsilon_\Lambda}} \left(\frac{\hbar^2}{2M_q} \right)^{3/2}$$

should coincide with the bare force in the 1S_0 channel.

A fit to the **experimental 1S_0 NN phase shifts** yields $\varepsilon_\Lambda \sim 7 - 8$ MeV.
Esbensen et al., Phys. Rev. C 56, 3054 (1997).



The fit to nuclear masses leads to a non monotonic dependence of the rms error on the cutoff.

Chamel et al., in "50 Years of Nuclear BCS" (World Scientific Publishing Company, 2013), pp.284-296

For the functionals BSk16-BS29, optimum mass fits were obtained with $\varepsilon_\Lambda \sim 16$ MeV, while we found $\varepsilon_\Lambda \sim 6.5$ MeV for BSk30-32.

Pairing gaps from contact interactions

The “weak-coupling approximation” provides an accurate expression of the pairing gaps in homogeneous matter from any given contact interaction:

$$\Delta = 2\mu \exp\left(\frac{2}{g(\mu)v_{\text{reg}}^{\pi}}\right)$$

μ is the chemical potential, $g(\mu)$ is the density of s. p. states and v_{reg}^{π} is a regularized interaction

$$\frac{1}{v_{\text{reg}}^{\pi}} = \frac{1}{v^{\pi}} + \frac{1}{v_{\Lambda}^{\pi}}$$
$$v_{\Lambda}^{\pi} = \frac{4}{g(\mu)\Lambda(\varepsilon_{\Lambda}/\mu)}$$

Other contributions to pairing in finite nuclei

Pairing in finite nuclei is not expected to be the same as in infinite nuclear matter because of

- **Coulomb and charge symmetry breaking effects,**
- **polarization effects in odd nuclei** (we use the equal filling approximation),
- **coupling to surface vibrations.**

Other contributions to pairing in finite nuclei

Pairing in finite nuclei is not expected to be the same as in infinite nuclear matter because of

- **Coulomb and charge symmetry breaking effects,**
- **polarization effects in odd nuclei** (we use the equal filling approximation),
- **coupling to surface vibrations.**

In an attempt to account for these effects, we include an additional phenomenological term in the pairing functional (only for BSk30-32)

$$v^{\pi q} \rightarrow v^{\pi q} + \kappa_q |\nabla n|^2$$

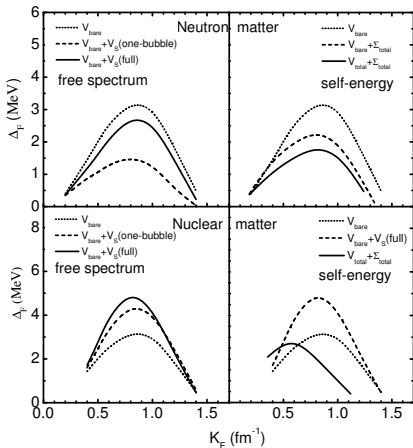
and we introduce renormalization factors f_q^\pm

$$v^{\pi q} \longrightarrow f_q^\pm v^{\pi q},$$

Typically $f_q^\pm \simeq 1 - 1.2$ and $f_q^- > f_q^+$, and $\kappa_q < 0$.

1S_0 pairing gaps in nuclear matter

For consistency, we considered the gaps obtained from extended BHF calculations since effective masses as well as equations of state have been also calculated with this approach.

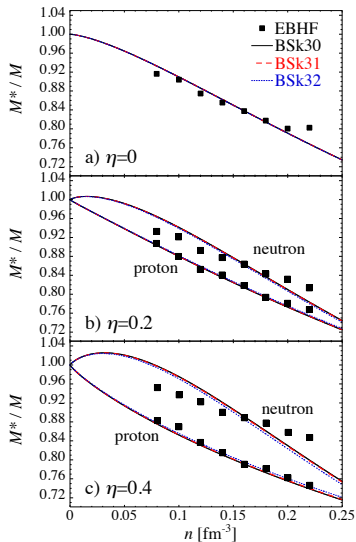


For comparison, we fitted functionals to different approximations for the gaps:

- **BCS:** BSk16
- **polarization+free spectrum:** BSk17-BSk29
- **polarization+self-energy:** BSk30-32.

*Cao et al.,
Phys.Rev.C74,064301(2006)*

Nucleon effective masses



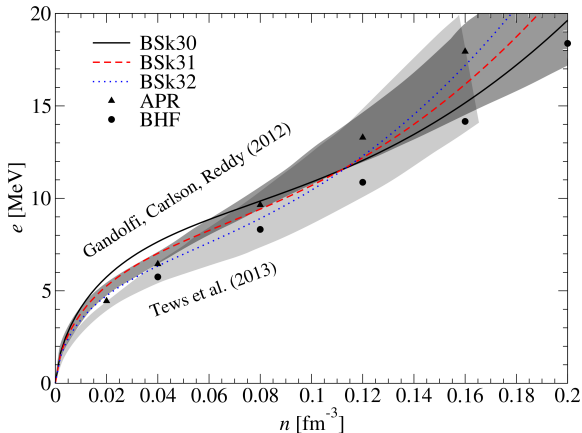
Effective masses obtained with our functionals are consistent with giant resonances in finite nuclei and many-body calculations in infinite nuclear matter.

This was achieved using **generalized Skyrme interactions** with density dependent t_1 and t_2 terms, initially introduced to remove spurious instabilities.
Chamel, Goriely, Pearson, Phys.Rev.C80,065804(2009)

EBHF calculations from *Cao et al., Phys.Rev.C73,014313(2006)*.

Neutron-matter equation of state

The neutron-matter equation of state obtained with our functionals are consistent with microscopic calculations using realistic interactions:



Applications to Neutron-Star Crusts

Description of neutron star crust below neutron drip

Main assumptions:

- atoms are fully pressure ionized $\rho \gg 10AZ \text{ g cm}^{-3}$
- the crust is a solid crystal
$$T < T_m \approx 1.3 \times 10^5 Z^2 \left(\frac{\rho_6}{A} \right)^{1/3} \text{ K} \quad \rho_6 \equiv \rho / 10^6 \text{ g cm}^{-3}$$
- electrons are uniformly distributed and are highly degenerate
$$T < T_F \approx 5.93 \times 10^9 (\gamma_r - 1) \text{ K}$$
$$\gamma_r \equiv \sqrt{1 + x_r^2}, \quad x_r \equiv \frac{\rho_F}{m_e c} \approx 1.00884 \left(\frac{\rho_6 Z}{A} \right)^{1/3}$$
- matter is fully catalyzed

The only microscopic inputs are nuclear masses. We have made use of the experimental data (Atomic Mass Evaluation) complemented with our HFB mass tables.

Pearson, Goriely, Chamel, Phys. Rev. C83, 065810 (2011).

Composition of the outer crust of a neutron star

Sequence of equilibrium nuclides with increasing depth:

HFB-30	HFB-31	HFB-32
⁵⁶ Fe	⁵⁶ Fe	⁵⁶ Fe
⁶² Ni	⁶² Ni	⁶² Ni
⁶⁴ Ni	⁶⁴ Ni	⁶⁴ Ni
⁶⁶ Ni	⁶⁶ Ni	⁶⁶ Ni
⁸⁶ Kr	⁸⁶ Kr	⁸⁶ Kr
⁸⁴ Se	⁸⁴ Se	⁸⁴ Se
⁸² Ge	⁸² Ge	⁸² Ge
⁸⁰ Zn	⁸⁰ Zn	⁸⁰ Zn
⁷⁸ Ni	⁷⁸ Ni	⁷⁸ Ni
⁸⁰ Ni	-	⁸⁰ Ni
¹²⁶ Ru	¹²⁶ Ru	-
¹²⁴ Mo	¹²⁴ Mo	¹²⁴ Mo
¹²² Zr	¹²² Zr	¹²² Zr
¹²¹ Y	¹²¹ Y	¹²¹ Y
¹²⁰ Sr	¹²⁰ Sr	¹²⁰ Sr
¹²² Sr	¹²² Sr	¹²² Sr
¹²⁴ Sr	-	¹²⁴ Sr

Predominance of even-even nuclei due to pairing.

Deeper (below ~ 200 m for a $1.4M_{\odot}$ neutron star with a 10 km radius) the composition is more model-dependent. Measurements of neutron-rich nuclei are crucially needed.

Pearson, Goriely, Chamel, Phys. Rev. C83, 065810.
Wolf et al., PRL 110, 041101.

Neutron-drip transition: general considerations

With increasing pressure, nuclei become progressively more neutron rich until neutrons start to drip out.

At this point, nuclei are actually stable against neutron emission but are unstable against *electron captures* accompanied by neutron emission ${}^A_Z X + \Delta Z e^- \rightarrow {}^{A-\Delta N}_{Z-\Delta Z} Y + \Delta N n + \Delta Z \nu_e$

Neutron-drip transition: general considerations

With increasing pressure, nuclei become progressively more neutron rich until neutrons start to drip out.

At this point, nuclei are actually stable against neutron emission but are unstable against *electron captures* accompanied by neutron emission ${}^A_Z X + \Delta Z e^- \rightarrow {}^{A-\Delta N}_{Z-\Delta Z} Y + \Delta N n + \Delta Z \nu_e$

- **nonaccreting neutron stars**

According to the cold catalyzed matter hypothesis, all kinds of reactions are allowed: the ground state is reached for $\Delta Z = Z$ and $\Delta N = A$.

- **accreting neutron stars**

Multiple electron captures are very unlikely therefore $\Delta Z = 1$ ($\Delta N \geq 1$). The dripping nucleus ${}^A_Z X$ is such that ${}^A_{Z-1} Y$ is unstable against neutron emission.

ρ_{drip} and P_{drip} can be expressed by simple analytical formulas.
Chamel, Fantina, Zdunik, Haensel, Phys. Rev. C91,055803(2015).

Neutron-drip transition in unmagnetized neutron stars

- **nonaccreting neutron stars**

	outer crust	drip line	ρ_{drip} (g cm^{-3})	P_{drip} (dyn cm^{-2})
HFB-19	^{126}Sr (0.73)	^{121}Sr (-0.62)	4.40×10^{11}	7.91×10^{29}
HFB-20	^{126}Sr (0.48)	^{121}Sr (-0.71)	4.39×10^{11}	7.89×10^{29}
HFB-21	^{124}Sr (0.83)	^{121}Sr (-0.33)	4.30×10^{11}	7.84×10^{29}

- **accreting neutron stars**

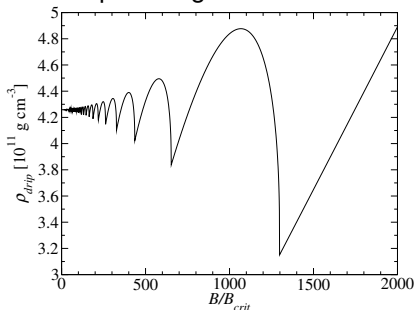
With HFB-21:

A	Z	ΔN	$\rho_{\text{drip-acc}}$ ($10^{11} \text{ g cm}^{-3}$)	$P_{\text{drip-acc}}$ ($10^{29} \text{ dyn cm}^{-2}$)
104	32	1	4.85	9.31
105	33	1	3.42	6.01
68	22	1	4.13	8.12
64	20	3	5.84	12.3
72	22	1	5.35	10.6
76	24	1	5.02	10.2
98	32	1	3.42	6.33
103	33	1	2.83	4.79
106	34	1	3.65	6.72
66	22	1	3.58	6.98
64	20	3	5.84	12.3
60	20	1	3.36	6.43

Neutron drip transition in magnetars

The neutron drip density exhibits typical quantum oscillations.

Example using HFB-24:



These oscillations are almost universal:

$$\frac{\rho_{\text{drip}}^{\text{min}}}{\rho_{\text{drip}}(B_{\star} = 0)} \approx \frac{3}{4}$$

$$\frac{\rho_{\text{drip}}^{\text{max}}}{\rho_{\text{drip}}(B_{\star} = 0)} \approx \frac{35 + 13\sqrt{13}}{72}$$

In the strongly quantizing regime,

$$\rho_{\text{drip}} \approx \frac{A}{Z} m \frac{\mu_e^{\text{drip}}}{m_e c^2} \frac{B_{\star}}{2\pi^2 \lambda_e^3} \left[1 - \frac{4}{3} C_{\alpha} Z^{2/3} \left(\frac{B_{\star}}{2\pi^2} \right)^{1/3} \left(\frac{m_e c^2}{\mu_e^{\text{drip}}} \right)^{2/3} \right]$$

Chamel et al., Phys.Rev.C91, 065801(2015).

Description of neutron star crust beyond neutron drip

Extended Thomas-Fermi+Strutinsky Integral (ETFSI) approach:

- $\tau_q(\mathbf{r})$ and $\mathbf{J}_q(\mathbf{r})$ are expanded into $n_q(\mathbf{r})$ and its gradients
- minimization of the energy yields

$$\lambda_q = \frac{\delta E}{\delta n_q(\mathbf{r})} \text{ whose solutions are } \widetilde{n}_q(\mathbf{r}) \text{ and } E[\widetilde{n}_q(\mathbf{r})] = E_{\text{ETF}}$$

- proton shell effects are added perturbatively using the Strutinsky integral theorem $E \approx E_{\text{ETF}} + \delta E_p$ (neutron shell effects are expected to be much smaller, $|\delta E_n| \ll |\delta E_p|$)

$$\delta E_p = \sum_k v_k^2 \varepsilon_k - \int d^3\mathbf{r} \left\{ \frac{\hbar^2}{2M_p^*(\mathbf{r})} \widetilde{\tau}_p(\mathbf{r}) + \widetilde{n}_p(\mathbf{r}) \widetilde{U}_p(\mathbf{r}) + \widetilde{\mathbf{J}}_p(\mathbf{r}) \cdot \widetilde{\mathbf{W}}_p(\mathbf{r}) \right\} - \sum_k \frac{\Delta_k^2}{4E_k}$$

$$\text{where } \left\{ -\nabla \cdot \frac{\hbar^2}{2M_p^*(\mathbf{r})} \nabla + \widetilde{U}_p(\mathbf{r}) - i \widetilde{\mathbf{W}}_p(\mathbf{r}) \cdot \nabla \times \boldsymbol{\sigma} \right\} \varphi_k(\mathbf{r}) = \varepsilon_k \varphi_k(\mathbf{r})$$

$$E_k = \sqrt{(\varepsilon_k - \lambda_p)^2 + \Delta_k^2}, \quad v_k^2 = \frac{1}{2} \left(1 - \frac{\varepsilon_k - \lambda_p}{E_k} \right)$$

$$\Delta_k = -\frac{1}{4} \sum_l \bar{v}_{k\bar{k},l}^{\text{pair}} \frac{\Delta_l}{E_l}$$

Description of neutron star crust beyond neutron drip

In order to further speed-up the calculations, we make the following approximations:

- neutron-proton clusters are spherical and $n_q(\mathbf{r})$ are parametrized as $n_q(\mathbf{r}) = n_{Bq} + n_{\Lambda q} f_q(r)$, where

$$f_q(r) = \frac{1}{1 + \exp \left\{ \left(\frac{C_q - R}{r - R} \right)^2 - 1 \right\} \exp \left(\frac{r - C_q}{a_q} \right)}$$

- the lattice energy is computed using the Wigner-Seitz method,
- electrons are uniformly distributed.

Pearson,Chamel,Pastore,Goriely,Phys.Rev.C91, 018801 (2015).

Pearson,Chamel,Goriely,Ducoin,Phys.Rev.C85,065803(2012).

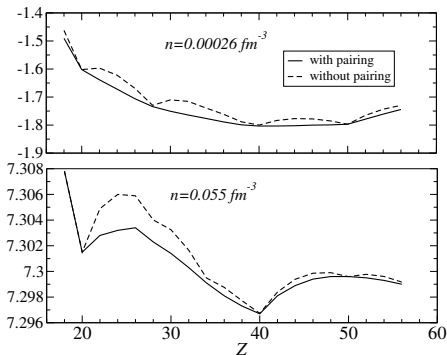
Advantages of the ETFSI method:

- very fast approximation to the full HF+BCS equations
- avoids the difficulties related to boundary conditions

Chamel et al.,Phys.Rev.C75(2007),055806.

Role of proton pairing on the composition of the inner crust of a neutron star

Proton shell effects are washed out due to pairing.



Example with BSk21.

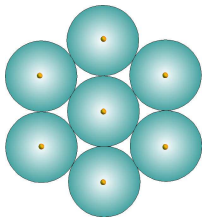
At low densities, $Z = 42$ is energetically favored over $Z = 40$, but by less than 5×10^{-4} MeV per nucleon.

A large range of values of Z could thus be present in a real neutron-star crust.

Pearson,Chamel,Pastore,Goriely,Phys.Rev.C91, 018801 (2015).

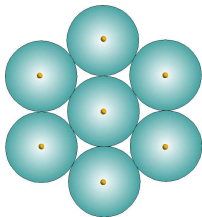
Due to proton pairing, the inner crust of a neutron star is expected to contain many impurities.

Neutron superfluidity in neutron-star crusts: Wigner-Seitz approach

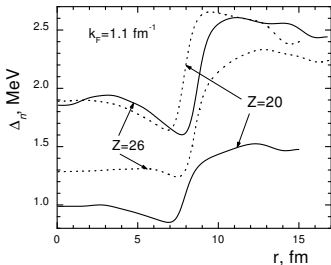


Superfluidity has been already studied with the HFB method using the Wigner-Seitz approximation. However, this approach breaks down in the deep region of the crust
Chamel et al., Phys.Rev.C75(2007)055806.

Neutron superfluidity in neutron-star crusts: Wigner-Seitz approach



Superfluidity has been already studied with the HFB method using the Wigner-Seitz approximation. However, this approach breaks down in the deep region of the crust
Chamel et al., Phys.Rev.C75(2007)055806.



Spurious shell effects $\propto 1/R^2$
can be very large at the crust
bottom and are enhanced by the
self-consistency.

Baldo et al., EPJA32,97(2007).

These limitations can be overcome by using the band theory of solids.

Band theory

Floquet-Bloch theorem

I found to my delight that the wave differed from the plane wave of free electrons only by a periodic modulation.

Bloch, Physics Today 29 (1976), 23-27.

Band theory

Floquet-Bloch theorem

I found to my delight that the wave differed from the plane wave of free electrons only by a periodic modulation.

Bloch, Physics Today 29 (1976), 23-27.



The single-particle wave functions can be expressed as

$$\varphi_{\alpha\mathbf{k}}(\mathbf{r}) = e^{i\mathbf{k}\cdot\mathbf{r}} u_{\alpha\mathbf{k}}(\mathbf{r})$$

where $u_{\alpha\mathbf{k}}(\mathbf{r} + \boldsymbol{\ell}) = u_{\alpha\mathbf{k}}(\mathbf{r})$ and $\boldsymbol{\ell}$ are lattice vectors.

Band theory

Floquet-Bloch theorem

I found to my delight that the wave differed from the plane wave of free electrons only by a periodic modulation.

Bloch, Physics Today 29 (1976), 23-27.



The single-particle wave functions can be expressed as

$$\varphi_{\alpha\mathbf{k}}(\mathbf{r}) = e^{i\mathbf{k}\cdot\mathbf{r}} u_{\alpha\mathbf{k}}(\mathbf{r})$$

where $u_{\alpha\mathbf{k}}(\mathbf{r} + \boldsymbol{\ell}) = u_{\alpha\mathbf{k}}(\mathbf{r})$ and $\boldsymbol{\ell}$ are lattice vectors.

- α (band index) accounts for the rotational symmetry around each lattice site,
- \mathbf{k} (wave vector) accounts for the translational symmetry of the crystal.

Chamel, Goriely, Pearson, in "50 years of Nuclear BCS" (World Scientific Publishing, 2013), pp.284-296.

Band theory

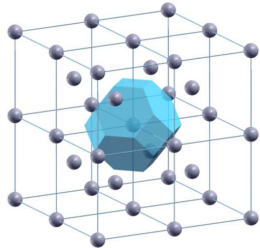
By symmetry, the crystal can be partitioned into identical primitive cells. The HFB equations need to be solved only inside one cell.

Band theory

By symmetry, the crystal can be partitioned into identical primitive cells. The HFB equations need to be solved only inside one cell.

- The shape of the cell depends on the crystal symmetry

Example : body centered
cubic lattice

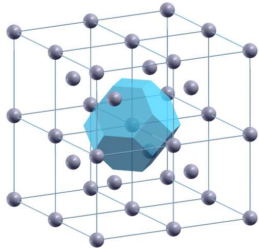


Band theory

By symmetry, the crystal can be partitioned into identical primitive cells. The HFB equations need to be solved only inside one cell.

- The shape of the cell depends on the crystal symmetry

Example : body centered cubic lattice



- The boundary conditions are fixed by the Floquet-Bloch theorem

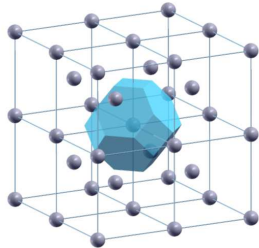
$$\varphi_{\alpha\mathbf{k}}(\mathbf{r} + \boldsymbol{\ell}) = e^{i\mathbf{k}\cdot\boldsymbol{\ell}} \varphi_{\alpha\mathbf{k}}(\mathbf{r})$$

Band theory

By symmetry, the crystal can be partitioned into identical primitive cells. The HFB equations need to be solved only inside one cell.

- The shape of the cell depends on the crystal symmetry

Example : body centered cubic lattice



- The boundary conditions are fixed by the Floquet-Bloch theorem

$$\varphi_{\alpha\mathbf{k}}(\mathbf{r} + \boldsymbol{\ell}) = e^{i\mathbf{k}\cdot\boldsymbol{\ell}} \varphi_{\alpha\mathbf{k}}(\mathbf{r})$$

- \mathbf{k} can be restricted to the first Brillouin zone (primitive cell of the reciprocal lattice) since for any reciprocal lattice vector \mathbf{K}

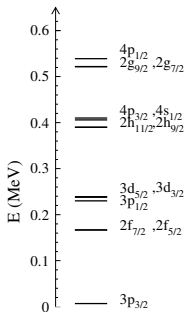
$$\varphi_{\alpha\mathbf{k}+\mathbf{K}}(\mathbf{r}) = \varphi_{\alpha\mathbf{k}}(\mathbf{r})$$

Example of neutron band structure

Discrete energy levels are replaced by energy bands in k -space.

Example: body-centered cubic crystal of zirconium like clusters with $N = 160$ (70 unbound) and $\bar{\rho} = 7 \times 10^{11} \text{ g.cm}^{-3}$

W-S approximation

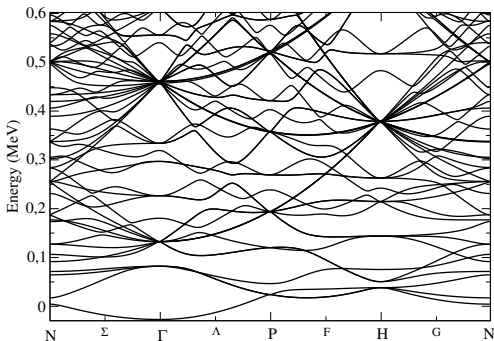
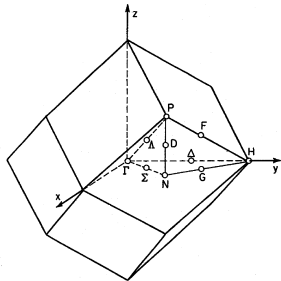


Example of neutron band structure

Discrete energy levels are replaced by energy bands in k -space.

Example: body-centered cubic crystal of zirconium like clusters with $N = 160$ (70 unbound) and $\bar{\rho} = 7 \times 10^{11} \text{ g.cm}^{-3}$

band theory



Neutron superfluidity in neutron-star crusts: band theory

In the deep layers of neutron-star crusts, the spatial fluctuations of $\Delta(\mathbf{r})$ are small compared to those of $\varphi_{\alpha\mathbf{k}}(\mathbf{r})$ so that

$$\int d^3\mathbf{r} \varphi_{\alpha\mathbf{k}}^*(\mathbf{r}) \Delta(\mathbf{r}) \varphi_{\beta\mathbf{k}}(\mathbf{r}) \approx \delta_{\alpha\beta} \int d^3\mathbf{r} |\varphi_{\alpha\mathbf{k}}(\mathbf{r})|^2 \Delta(\mathbf{r}).$$

Neutron superfluidity in neutron-star crusts: band theory

In the deep layers of neutron-star crusts, the spatial fluctuations of $\Delta(\mathbf{r})$ are small compared to those of $\varphi_{\alpha\mathbf{k}}(\mathbf{r})$ so that

$$\int d^3\mathbf{r} \varphi_{\alpha\mathbf{k}}^*(\mathbf{r})\Delta(\mathbf{r})\varphi_{\beta\mathbf{k}}(\mathbf{r}) \approx \delta_{\alpha\beta} \int d^3\mathbf{r} |\varphi_{\alpha\mathbf{k}}(\mathbf{r})|^2 \Delta(\mathbf{r}).$$

In this decoupling approximation, the Hartree-Fock-Bogoliubov equations reduce to the **multi-band BCS equations**:

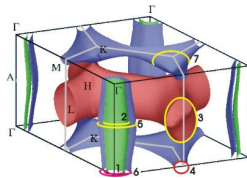
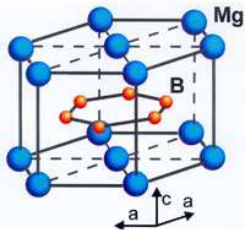
$$\Delta_{\alpha\mathbf{k}} = -\frac{1}{2} \sum_{\beta} \int \frac{d^3\mathbf{k}'}{(2\pi)^3} \bar{v}_{\alpha\mathbf{k}\alpha-\mathbf{k}\beta\mathbf{k}'\beta-\mathbf{k}'}^{\text{pair}} \frac{\Delta_{\beta\mathbf{k}'}}{E_{\beta\mathbf{k}'}} \tanh \frac{E_{\beta\mathbf{k}'}}{2k_{\text{B}}T}$$
$$\bar{v}_{\alpha\mathbf{k}\alpha-\mathbf{k}\beta\mathbf{k}'\beta-\mathbf{k}'}^{\text{pair}} = \int d^3\mathbf{r} v^{\pi}[\rho_n(\mathbf{r}), \rho_p(\mathbf{r})] |\varphi_{\alpha\mathbf{k}}(\mathbf{r})|^2 |\varphi_{\beta\mathbf{k}'}(\mathbf{r})|^2$$
$$E_{\alpha\mathbf{k}} = \sqrt{(\varepsilon_{\alpha\mathbf{k}} - \mu)^2 + \Delta_{\alpha\mathbf{k}}^2}$$

$\varepsilon_{\alpha\mathbf{k}}$, μ and $\varphi_{\alpha\mathbf{k}}(\mathbf{r})$ are obtained from band structure calculations using the ETFSI mean fields

Chamel et al., Phys.Rev.C81,045804 (2010).

Analogy with terrestrial multi-band superconductors

Multi-band superconductors were first studied by Suhl et al. in 1959 but clear evidence were found only in 2001 with the discovery of MgB_2 (two-band superconductor)



In neutron-star crusts,

- the number of bands can be huge \sim up to a thousand!
- both intra- and inter-band couplings must be taken into account

Neutron pairing gaps

Results obtained for BSk16

n_n^f is the density of unbound neutrons

Δ_u is the gap in neutron matter at density n_n^f

$\bar{\Delta}_u$ is the gap in neutron matter at density n_n

\bar{n} [fm^{-3}]	Z	A	n_n^f [fm^{-3}]	Δ_F [MeV]	Δ_u [MeV]	$\bar{\Delta}_u$ [MeV]
0.07	40	1218	0.060	1.44	1.79	1.43
0.065	40	1264	0.056	1.65	1.99	1.65
0.06	40	1260	0.051	1.86	2.20	1.87
0.055	40	1254	0.047	2.08	2.40	2.10
0.05	40	1264	0.043	2.29	2.59	2.33

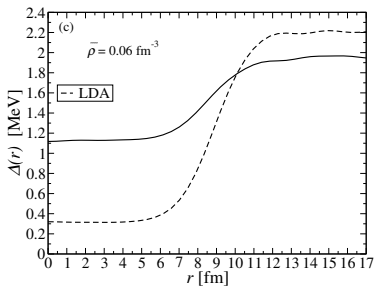
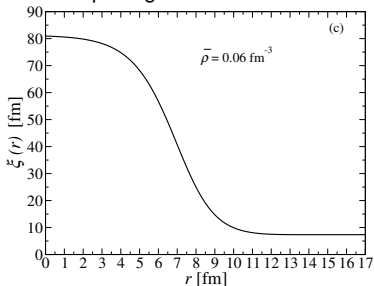
- $\Delta_{\alpha\mathbf{k}}(T)/\Delta_{\alpha\mathbf{k}}(0)$ is a universal function of T
- The critical temperature is approximately given by the usual BCS relation $T_c \simeq 0.567\Delta_F$
- the nuclear clusters lower the gap by 10 – 20%

Pairing field and local density approximation

The effects of inhomogeneities on neutron superfluidity can be directly seen in the pairing field

$$\Delta_n(\mathbf{r}) = -\frac{1}{2} v^{\pi n} [n_n(\mathbf{r}), n_p(\mathbf{r})] \sum_{\alpha} \int \frac{d^3 \mathbf{k}}{(2\pi)^3} |\varphi_{\alpha \mathbf{k}}(\mathbf{r})|^2 \frac{\Delta_{\alpha \mathbf{k}}}{E_{\alpha \mathbf{k}}}$$

Neutron pairing field for $\bar{n} = 0.06 \text{ fm}^{-3}$ at $T = 0$:



The superfluid permeates the clusters due to proximity effects.

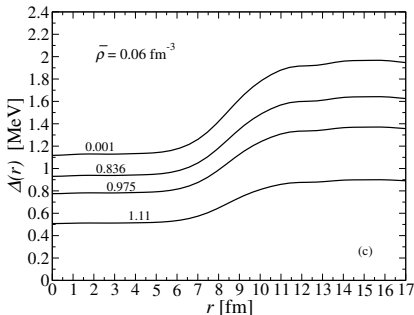
Pairing field at finite temperature

The neutron pairing field is now given by

$$\Delta_n(\mathbf{r}) = -\frac{1}{2}v^{\pi n}[n_n(\mathbf{r}), n_p(\mathbf{r})]\tilde{n}_n(\mathbf{r}), \quad \tilde{n}_n(\mathbf{r}) = \sum_{\alpha, \mathbf{k}}^{\Lambda} |\varphi_{\alpha \mathbf{k}}(\mathbf{r})|^2 \frac{\Delta_{\alpha \mathbf{k}}}{E_{\alpha \mathbf{k}}} \tanh \frac{E_{\alpha \mathbf{k}}}{2T}$$

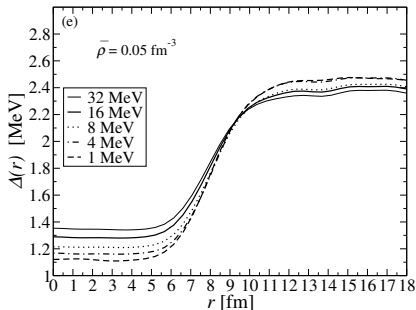
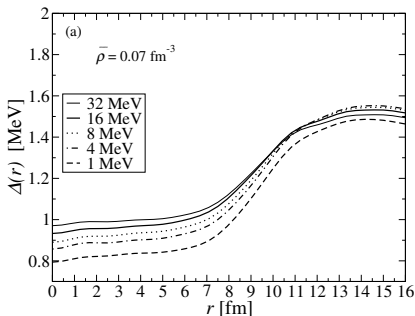
Neutron pairing field for $\bar{n} = 0.06 \text{ fm}^{-3}$:

The superfluid becomes more and more homogeneous as T approaches T_c



Chamel et al., *Phys.Rev.C*81(2010)045804.

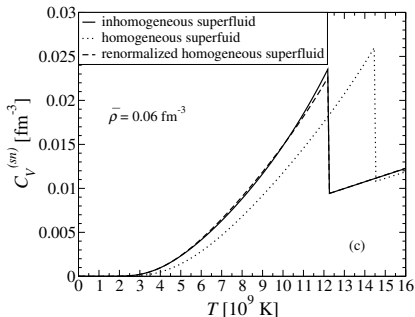
Impact of the pairing cutoff



\bar{n} [fm ⁻³]	$\Delta_{F0}(16)$ [MeV]	$\Delta_{F0}(8)$	$\Delta_{F0}(4)$	$\Delta_{F0}(2)$	$\Delta_{F0}(1)$
0.070	1.39	1.38	1.37	1.36	1.29
0.050	2.27	2.25	2.27	2.26	2.24

Pairing gaps (hence also critical temperatures) are very weakly dependent on the pairing cutoff.

Impact on thermodynamic quantities : specific heat



The neutron specific heat is exponentially suppressed at $T < T_c$ as in pure neutron matter.

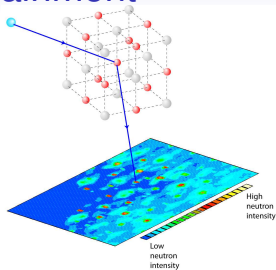
- Band structure effects are small (id. for normal neutrons).
Chamel et al, Phys. Rev. C 79, 012801(R) (2009)
- The renormalization of T_c comes from the density dependence of the pairing strength.
Chamel et al., Phys.Rev.C81(2010)045804.

Generic interpolating formula valid for any temperature:
Pastore, Chamel, Margueron, MNRAS 448, 1887 (2015).

Bragg scattering and entrainment

For decades, neutron diffraction experiments have been routinely performed to explore the structure of materials.

The main difference in neutron-star crusts is that **neutrons are highly degenerate**



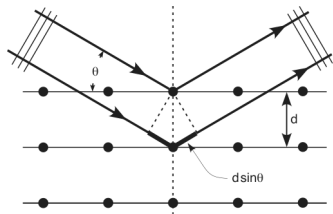
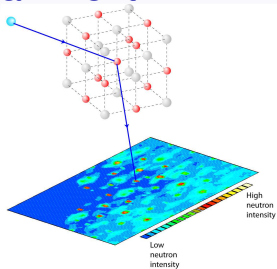
Bragg scattering and entrainment

For decades, neutron diffraction experiments have been routinely performed to explore the structure of materials.

The main difference in neutron-star crusts is that **neutrons are highly degenerate**

A neutron with wavevector \mathbf{k} can be **coherently scattered** if $d \sin \theta = N\pi/k$, where $N = 0, 1, 2, \dots$ (Bragg's law).

In this case, it does not propagate in the crystal: it is therefore entrained!



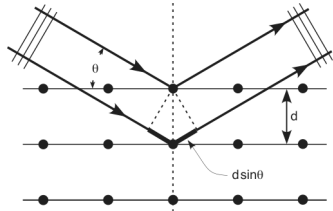
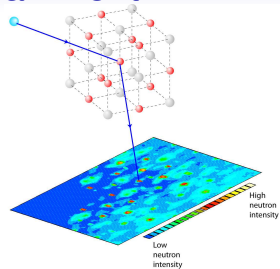
Bragg scattering and entrainment

For decades, neutron diffraction experiments have been routinely performed to explore the structure of materials.

The main difference in neutron-star crusts is that **neutrons are highly degenerate**

A neutron with wavevector \mathbf{k} can be **coherently scattered** if $d \sin \theta = N\pi/k$, where $N = 0, 1, 2, \dots$ (Bragg's law).

In this case, it does not propagate in the crystal: it is therefore entrained!



Bragg scattering occurs if $k > \pi/d$. In neutron stars, neutrons have momenta up to k_F . Typically $k_F > \pi/d$ in all regions of the inner crust but the shallowest.

How “free” are neutrons in neutron-star crusts?

Only some “conduction” neutrons contribute to the neutron current:

$$n_n^c = \frac{m_n}{24\pi^3\hbar^2} \sum_{\alpha} \int_F |\nabla_{\mathbf{k}} \varepsilon_{\alpha\mathbf{k}}| dS^{(\alpha)} \leq n_n^f, \quad m_n^* = m_n \frac{n_n^f}{n_n^c} \geq m_n$$

Chamel, PhD thesis, Université Paris 6, France (2004)

Carter, Chamel, Haensel, Nucl. Phys. A748, 675 (2005)

Pethick, Chamel, Reddy, Prog.Theor.Phys.Sup.186(2010)9.

\bar{n} (fm ⁻³)	n_n^f/n_n (%)	n_n^c/n_n^f (%)
0.0003	20.0	82.6
0.001	68.6	27.3
0.005	86.4	17.5
0.01	88.9	15.5
0.02	90.3	7.37
0.03	91.4	7.33
0.04	88.8	10.6
0.05	91.4	30.0
0.06	91.5	45.9

\bar{n} is the average baryon density

n_n is the total neutron density

n_n^f is the “free” neutron density

n_n^c is the “conduction” neutron density

In many layers, most neutrons are entrained by the crust!

Chamel, Phys.Rev.C85,035801(2012)

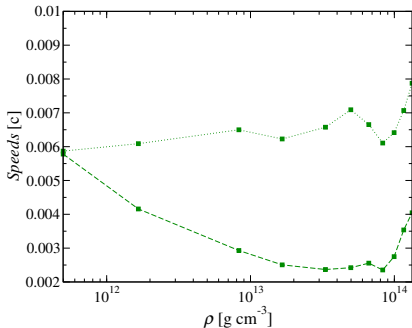
Entrainment and collective excitations

Entrainment impacts low-energy collective excitations:

- clusters are effectively heavier,
- longitudinal excitations are mixed.

Chamel, Page, Reddy, Phys. Rev. C 87, 035803 (2013)

Chamel, Page, Reddy, J. Phys. Conf. Ser. 665, 012065 (2016).



Transverse lattice phonon speeds with (dashed line) and without (dotted line) entrainment.

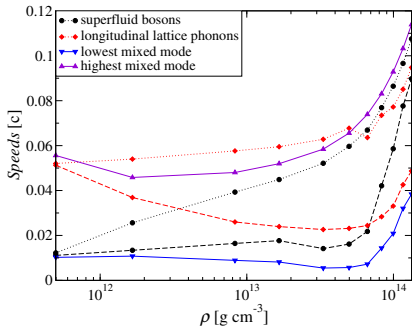
Entrainment and collective excitations

Entrainment impacts low-energy collective excitations:

- it makes clusters heavier,
- it mixes longitudinal excitations.

Chamel, Page, Reddy, Phys. Rev. C 87, 035803 (2013)

Chamel, Page, Reddy, J. Phys. Conf. Ser. 665, 012065 (2016).

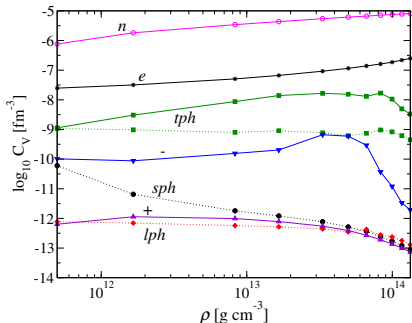


Longitudinal phonon speeds with (dashed line) and without (dotted line) entrainment but no mixing. Solids lines include entrainment and mixing.

Entrainment and thermal properties

The contribution of collective excitations to the specific heat at low T varies like $(k_B T / \hbar v)^3$. Since entrainment reduces v , the specific heat is enhanced.

Contributions to the crustal specific heat at $T = 10^7$ K :



n normal neutrons

e electrons

tph transverse lattice phonons

lph longitudinal lattice phonons
(without mixing)

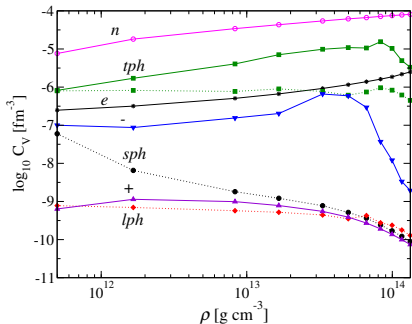
sph superfluid phonons (without
mixing)

\pm longitudinal mixed modes

Entrainment and thermal properties

The contribution of collective excitations to the specific heat at low T varies like $(k_B T / \hbar v)^3$. Since entrainment reduces v , the specific heat is enhanced.

Contributions to the crustal specific heat at $T = 10^8$ K :



n normal neutrons

e electrons

tph transverse lattice phonons

lph longitudinal lattice phonons
(without mixing)

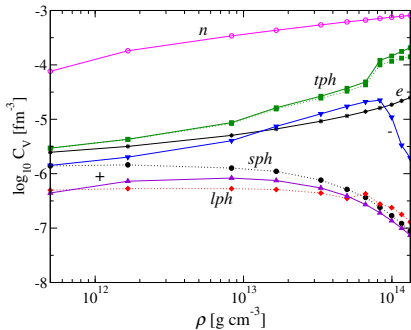
sph superfluid phonons (without
mixing)

\pm longitudinal mixed modes

Entrainment and thermal properties

The contribution of collective excitations to the specific heat at low T varies like $(k_B T / \hbar \nu)^3$. Since entrainment reduces ν , the specific heat is enhanced.

Contributions to the crustal specific heat at $T = 10^9$ K :



n normal neutrons

e electrons

tph transverse lattice phonons

lph longitudinal lattice phonons
(without mixing)

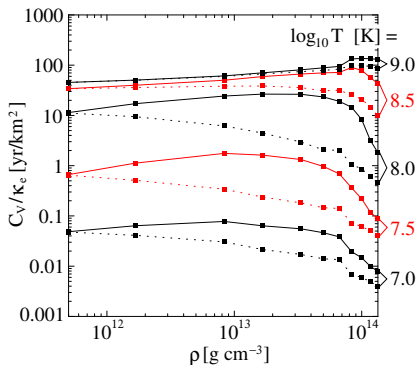
sph superfluid phonons (without
mixing)

± longitudinal mixed modes

Entrainment and thermal properties

Changes in phonon velocities alter the electron-phonon scattering hence also the (electron) thermal conductivity.

All in all, entrainment leads to an increase of the thermal relaxation time of the crust.



Thermal properties were calculated for catalyzed crusts; they may be different for accreted crusts.

Conclusions&Perspectives

OUTER LAYER
1 meter thick
solid or liquid

CORE
10-15 kilometer deep
liquid

We have developed a series of accurately calibrated nuclear energy density functionals with an improved treatment of pairing (BSk30-32).

These functionals are well-suited for describing extreme astrophysical environments like neutron stars.

Due to proton pairing, the crust of a neutron star is likely to contain an admixture of various kinds of nuclei.

Spatial inhomogeneities have a substantial impact on neutron superfluidity in the inner crust (entrainment).

Perspectives: role of neutron pairing on the crust structure, role of impurities and defects on neutron superfluidity, transport properties.

CRUST
1 kilometer thick
solid

NEUTRON STAR

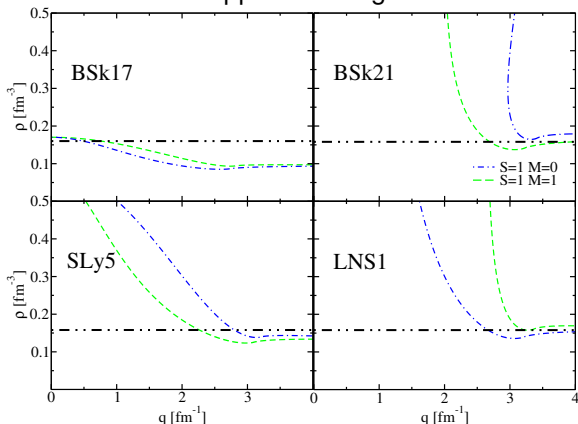
Spin and spin-isospin instabilities

BSk18-32 are devoid of spurious long-wavelength instabilities.

Chamel, Goriely, Pearson, Phys.Rev.C80,065804(2009)

Chamel & Goriely, Phys.Rev.C82, 045804 (2010)

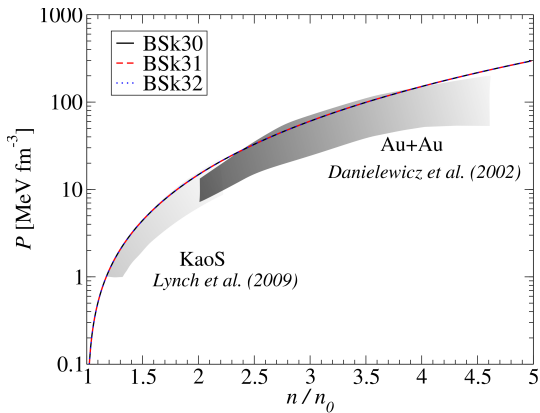
Finite-size instabilities are suppressed: e.g. neutron matter



Pastore et al., Phys.Rev.C90, 025804 (2014)

Symmetric nuclear-matter equation of state

Our functionals are also in good agreement with empirical constraints inferred from heavy-ion collisions:



Danielewicz et al., Science 298, 1592 (2002)

Lynch et al., Prog. Part. Nuc. Phys.62, 427 (2009)

Symmetry energy

The values for the symmetry energy J and its slope L obtained with our functionals are consistent with various experimental constraints (the dashed line delimits the values from 30 different HFB atomic mass models with rms < 0.84 MeV)

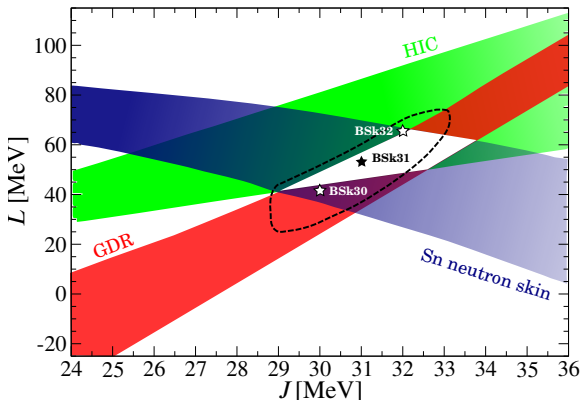


Figure adapted from *Lattimer & Steiner, EPJA50,40(2014)*

Latest Brussels-Montreal Skyrme functionals

The latest functionals BSk30-32 were fitted to 2353 nuclear masses from the 2012 Atomic Mass Evaluation with $Z, N \geq 8$ following the same protocols but with different symmetry energy coefficients J :

	HFB-30	HFB-31	HFB-32
J [MeV]	30	31	32
$\sigma(M)$ [MeV]	0.573	0.571	0.586
$\bar{\epsilon}(M)$ [MeV]	0.003	-0.004	-0.007
$\sigma(M_{nr})$ [MeV]	0.683	0.659	0.700
$\bar{\epsilon}(M_{nr})$ [MeV]	0.038	-0.015	0.137
$\sigma(R_C)$ [fm]	0.026	0.027	0.027
$\bar{\epsilon}(R_C)$ [fm]	0.001	0.002	0.000

<http://www.astro.ulb.ac.be/bruslib/>